Structural origin of the 15 μm residual absorption in the $BaGa_4Se_7$ crystal

Shengjie Jiang,[ab] *Songming Wan*,*[abd] *Wen Luo*,[a] *Bin Li*[ab] *and Jiyong Yao*[c]

[a] Anhui Provincial Key Laboratory of Photonics Devices and Materials, Anhui Institute of Optics and Fine Mechanics, HFIPS, Chinese Academy of Sciences, Hefei 230031, China

[b] University of Science and Technology of China, Hefei 230026, China

[c] Key Laboratory of Functional Crystals and Laser Technology, Technical Institute of Physics and Chemistry, Chinese Academy of Sciences, Beijing 100190, China

[d] Advanced Laser Technology Laboratory of Anhui Province, Hefei 230037, China

Table of Contents

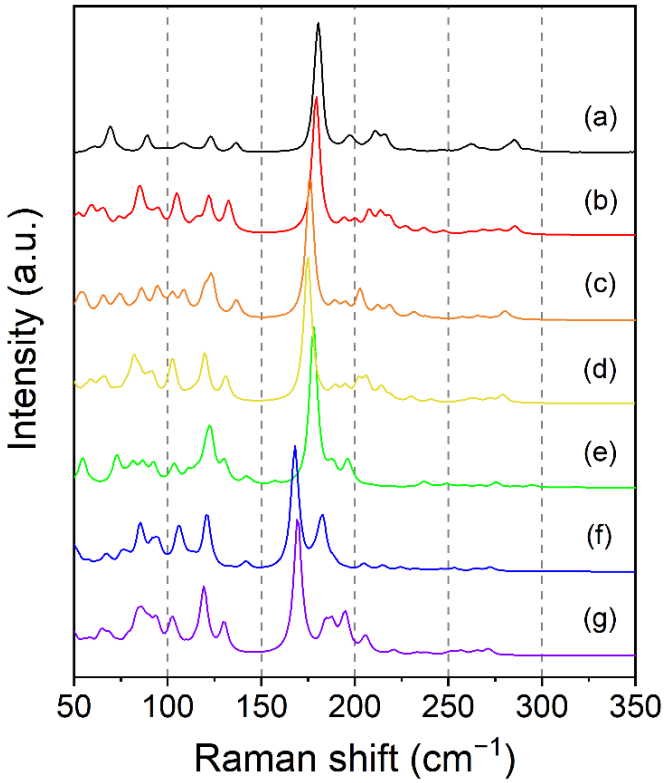

Figure S1. Raman spectra of the $BaGa_4Se_7$ crystal. (a) An experimental spectrum and (b–g) computational spectra with different exchange–correlation functional: (b) LDA-CA-PZ, (c) GGA-WC, (d) GGA-PBESOL, (e) GGA-PW91, (f) GGA-RPBE, and (g) GGA-PBE. All of the computations were performed with an energy cutoff of 950 eV and a *k*-point grid of 2 × 2 × 1. The computational Raman lines were broadened by a Lorentz line-shape function with a full width at half-maximum of 5 cm^{-1}.

Exchange–correlation functional is the most important parameter in DFT computations. Local (LDA) and semilocal (GGA) approximations are the most commonly applied type of exchange–correlation functional for solids. In order to select a suitable exchange–correlation functional, all of the LDA and GGA functionals provided in CASTEP (LDA-CA-PZ, GGA-WC, GGA-PBESOL, GGA-PW91, GGA-RPBE and GGA-PBE) were employed to simulate the Raman spectrum of the $BaGa_4Se_7$ crystal. As shown in Figure S1, the LDA-CA-PZ functional produces the optimal computational spectrum and was thus adopted in our work.

Table S1. Convergence test for the total energy of the $BaGa_4Se_7$ crystal with respect to the Γ-centered *k*-point grid (the energy cutoff is fixed at 1100 eV)

k-point	Total energy (eV)
1 × 1 × 1	−18649.91976
1 × 2 × 1	−18650.59684
2 × 2 × 1	−18654.36731
2 × 2 × 2	−18654.36952
2 × 3 × 2	−18654.33216

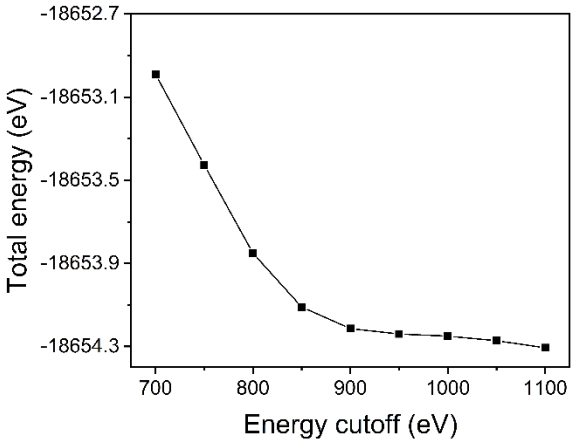

Figure S2. Convergence test for the total energy of the $BaGa_4Se_7$ crystal with respect to the energy cutoff (the Γ-centered *k*-point grid is fixed at 2 × 2 × 1).

Table S1 and Figure S2 present the results of convergence tests for the total energy of the $BaGa_4Se_7$ crystal with respect to the Γ-centered *k*-point grid and the energy cutoff. The results show that a Γ-centered *k*-point grid of 2 × 2 × 1 and an energy cutoff of 950 eV are sufficient to yield a converged total energy.

Table S2. Factor group analysis of the phonons of the perfect $BaGa_4Se_7$ crystal

Cs	*E*	$\sigma(xy)$	*N*	*T*	*T′*	*R′*	*n*	*Function*
A′	1	1	36	2	4	3	27	$x, z, x^2, y^2, z^2, xz, J_y$
A″	1	−1	36	1	5	3	27	y, xy, yz, J_x, J_z
$N_R(N)$	24	0						
$N_R(s)$	4	0						
$N_R(s-v)$	2	0						
$\chi_R(N)$	72	0						
$\chi_R(T)$	3	1						
$\chi_R(T')$	9	−1						
$\chi_R(R')$	6	0						
$\chi_R(n)$	54	0						

$N_R(N)$, $N_R(s)$, and $N_R(s-v)$ represent the numbers of total atoms, $Ga_4Se_7^{2-}$ groups plus Ba^{2+} cations, and $Ga_4Se_7^{2-}$ groups in the $BaGa_4Se_7$ unit cell, respectively. The centers of these atoms, groups, and cations remain invariant under the symmetry operations *R* (identity operation *E* and mirror plane operations $\sigma(xy)$). $\chi_R(N) = N_R(N)\cdot[\pm(1 + 2\cos\theta)]$, $\chi_R(T) = \pm(1 + 2\cos\theta)$, $\chi_R(T') = [N_R(s) - 1]\cdot[\pm(1 + 2\cos\theta)]$, $\chi_R(R') = N_R(s-v)\cdot[\pm(1 + 2\cos\theta)]$, and $\chi_R(n) = \chi_R(N) - \chi_R(T) - \chi_R(T') - \chi_R(R')$ are the characters of reducible representations. *N*, *T*, *T′*, *R′*, and *n* represent the total phonons, the translational phonons of the $BaGa_4Se_7$ unit cell as a whole (that is acoustic phonons), the remaining translational phonons, the librational phonons, and the internal vibrational phonons, respectively.

Table S3. Atom positions in the experimental and optimized $BaGa_4Se_7$ unit cells

Atom	*x/a*		*y/b*		*z/c*	
	Experimental	Optimized	Experimental	Optimized	Experimental	Optimized
Ba	0.5639	0.5667	0.3535	0.3540	0.0463	0.0485
Ga1	0.0072	0.0052	0.1659	0.1665	0.7408	0.7402
Ga2	1.0000	0.9966	0.0072	0.0059	1.0000	0.9996
Ga3	0.4927	0.4972	0.1583	0.1598	0.7280	0.7281
Ga4	0.2374	0.2390	0.3632	0.3620	0.2252	0.2258
Se1	0.7824	0.7685	0.1506	0.1482	0.5532	0.5508
Se2	0.0059	0.0016	0.3633	0.3667	0.0388	0.0367
Se3	0.3285	0.3314	0.1099	0.1130	0.5422	0.5409
Se4	0.3294	0.3341	0.0178	0.0154	0.3097	0.3110
Se5	0.0973	0.0955	0.5080	0.5051	0.3233	0.3245
Se6	0.5703	0.5805	0.4948	0.4906	0.2806	0.2826
Se7	0.8169	0.8189	0.0307	0.0391	0.3040	0.3034

Table S4. Computational phonon modes and their frequencies of the perfect $BaGa_4Se_7$ crystal

No.	Mode	ω/cm^{-1}	No.	Mode	ω/cm^{-1}	No.	Mode	ω/cm^{-1}
1	*A*″	−2.0	25	*A*″	89.2	49	*A*′	213.8
2	*A*′	0.0	26	*A*′	90.6	50	*A*″	216.0
3	*A*′	0.0	27	*A*″	90.8	51	*A*′	218.7
4	*A*″	0.0	28	*A*′	93.6	52	*A*″	227.0
5	*A*′	22.0	29	*A*″	95.5	53	*A*′	227.1
6	*A*″	36.5	30	*A*′	104.6	54	*A*″	227.9
7	*A*′	38.1	31	*A*′	105.9	55	*A*′	236.8
8	*A*′	43.7	32	*A*″	106.7	56	*A*″	238.1
9	*A*″	46.0	33	*A*″	107.5	57	*A*″	246.0
10	*A*′	47.6	34	*A*″	111.8	58	*A*′	247.5
11	*A*′	52.5	35	*A*″	114.3	59	*A*′	253.5
12	*A*″	52.7	36	*A*′	115.9	60	*A*″	257.4
13	*A*′	58.1	37	*A*″	117.6	61	*A*′	261.3
14	*A*″	59.8	38	*A*′	122.0	62	*A*″	262.2
15	*A*′	64.0	39	*A*″	127.5	63	*A*′	266.9
16	*A*″	64.4	40	*A*′	132.6	64	*A*″	268.7
17	*A*′	66.4	41	*A*″	174.4	65	*A*′	269.2
18	*A*″	69.1	42	*A*′	179.3	66	*A*″	273.6
19	*A*″	73.6	43	*A*″	186.0	67	*A*″	276.7
20	*A*′	74.3	44	*A*″	192.9	68	*A*′	277.1
21	*A*″	79.1	45	*A*′	194.3	69	*A*″	277.7
22	*A*′	84.3	46	*A*″	197.6	70	*A*′	285.4
23	*A*″	85.0	47	*A*′	200.1	71	*A*′	286.0
24	*A*′	85.6	48	*A*′	207.7	72	*A*″	294.8

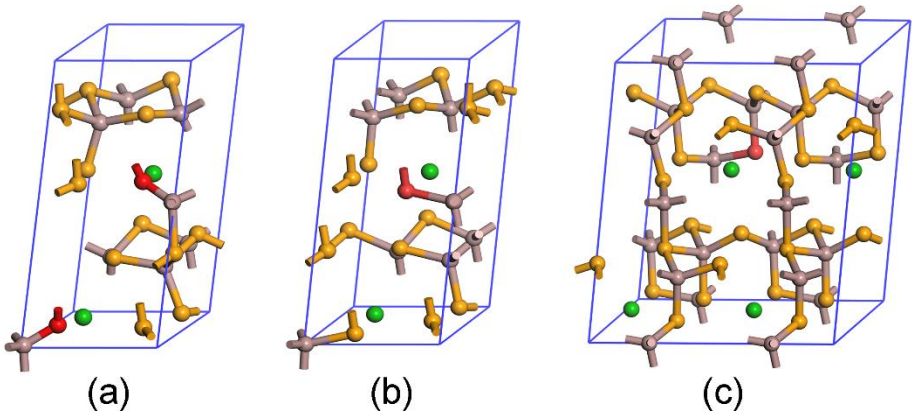

Figure S3. Three structural models for the O_{se2} defect crystal: (a) an unit cell with *Pc* symmetry, (b) an unit cell with *P*1 symmetry, and (c) a 1 × 2 × 1 supercell with *P*1 symmetry.

In order to demonstrate the rationality of the unit cell models, we established three unit cell/supercell models with different defect concentrations for the O_{se2} defect crystal. The first model, as described in the main article, has a defect concentration of 14.3% (O/(O + Se), Figure S3a). The second model was constructed by replacing a Se2 atom with an O atom in a *P*1 unit cell (the crystal symmetry had been converted to *P*1 before the replacement), which has a defect concentration of 7.14% (Figure S3b). The third model, with a defect concentration of 3.57%, was constructed by replacing a Se2 atom with an O atom in a 1 × 2 × 1 supercell with *P*1 symmetry (Figure S3c). Their computational IR and Raman spectra are shown in Figures S4 and S5. All of the computational wavelengths of the residual absorption are located at around 15 μm, independent of the cell size and the defect concentration. Therefore, the unit cell models used in this paper are appropriate.

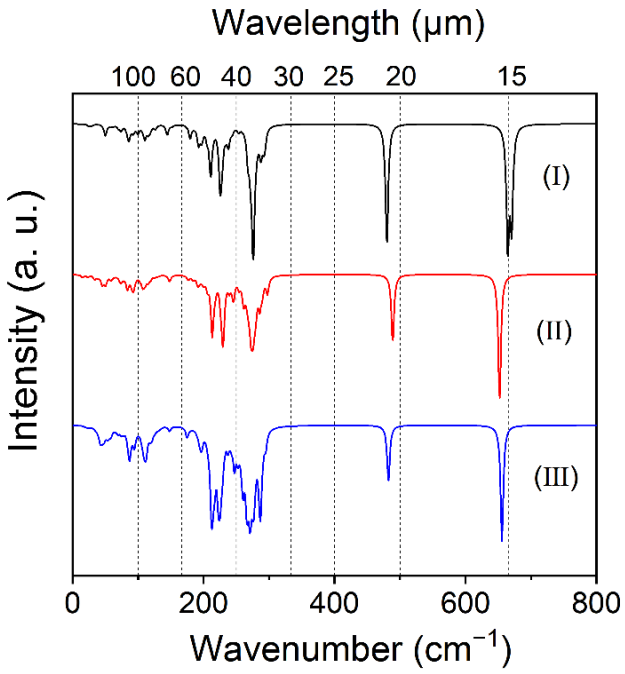

Figure S4. Computational IR spectra for three O_{Se2} defect crystals: (I) an unit cell with *Pc* symmetry, (II) an unit cell with *P*1 symmetry, and (III) a 1 × 2 × 1 supercell with *P*1 symmetry.

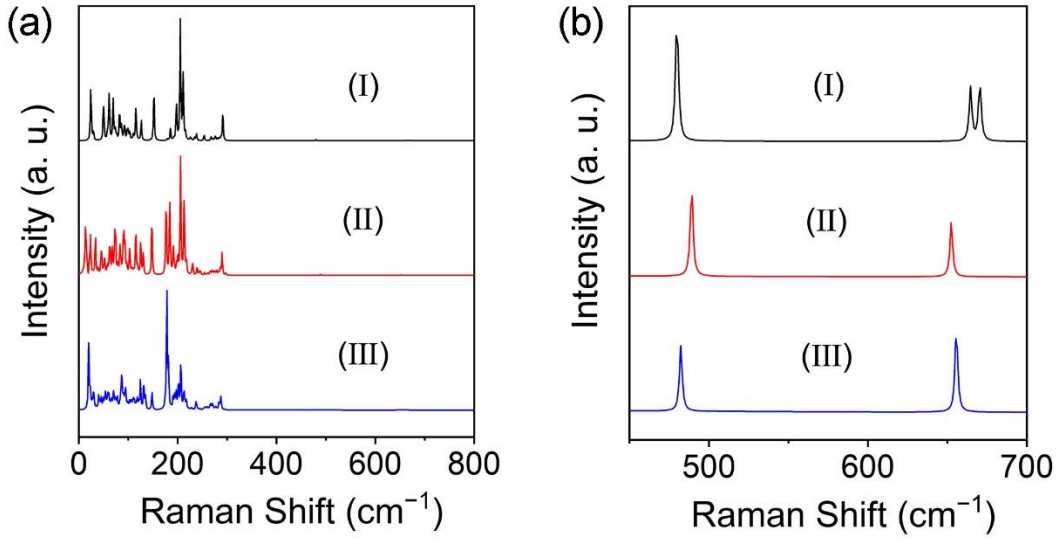

Figure S5. Computational Raman spectra for three O_{Se2} defect crystals in the range of (a) 0−800 cm^{-1} and (b) 450−700 cm^{-1}: (I) an unit cell with *Pc* symmetry, (II) an unit cell with *P*1 symmetry, and (III) a 1 × 2 × 1 supercell with *P*1 symmetry.

Table S5. Computational phonon modes and their frequencies of the O_{Se2} defect crystal

No.	Mode	ω/cm^{-1}	No.	Mode	ω/cm^{-1}	No.	Mode	ω/cm^{-1}
1	*A′*	0.0	25	*A′*	92.9	49	*A′*	225.3
2	*A″*	0.0	26	*A″*	97.6	50	*A″*	226.2
3	*A′*	0.0	27	*A′*	99.9	51	*A″*	228.2
4	*A′*	24.2	28	*A″*	102.8	52	*A′*	233.9
5	*A″*	26.3	29	*A′*	103.1	53	*A′*	238.0
6	*A″*	29.6	30	*A′*	107.3	54	*A″*	243.6
7	*A′*	49.3	31	*A″*	110.4	55	*A′*	253.5
8	*A′*	50.4	32	*A″*	115.1	56	*A″*	259.0
9	*A″*	57.4	33	*A′*	115.4	57	*A″*	267.2
10	*A′*	57.9	34	*A″*	118.5	58	*A′*	267.4
11	*A″*	60.2	35	*A″*	122.0	59	*A′*	267.9
12	*A′*	61.3	36	*A′*	126.3	60	*A″*	272.0
13	*A″*	61.6	37	*A″*	144.6	61	*A′*	275.7
14	*A′*	69.1	38	*A′*	151.9	62	*A″*	277.0
15	*A″*	69.8	39	*A″*	179.4	63	*A′*	280.7
16	*A″*	73.0	40	*A′*	185.3	64	*A″*	281.4
17	*A′*	74.0	41	*A″*	192.2	65	*A″*	284.5
18	*A′*	76.6	42	*A″*	196.1	66	*A′*	287.6
19	*A′*	82.4	43	*A′*	197.5	67	*A′*	291.4
20	*A″*	83.1	44	*A′*	205.3	68	*A″*	293.4
21	*A″*	85.2	45	*A″*	210.3	69	*A′*	479.7
22	*A′*	86.4	46	*A′*	211.0	70	*A″*	480.8
23	*A″*	90.1	47	*A′*	215.7	71	*A′*	664.6
24	*A″*	91.8	48	*A″*	223.7	72	*A″*	670.4

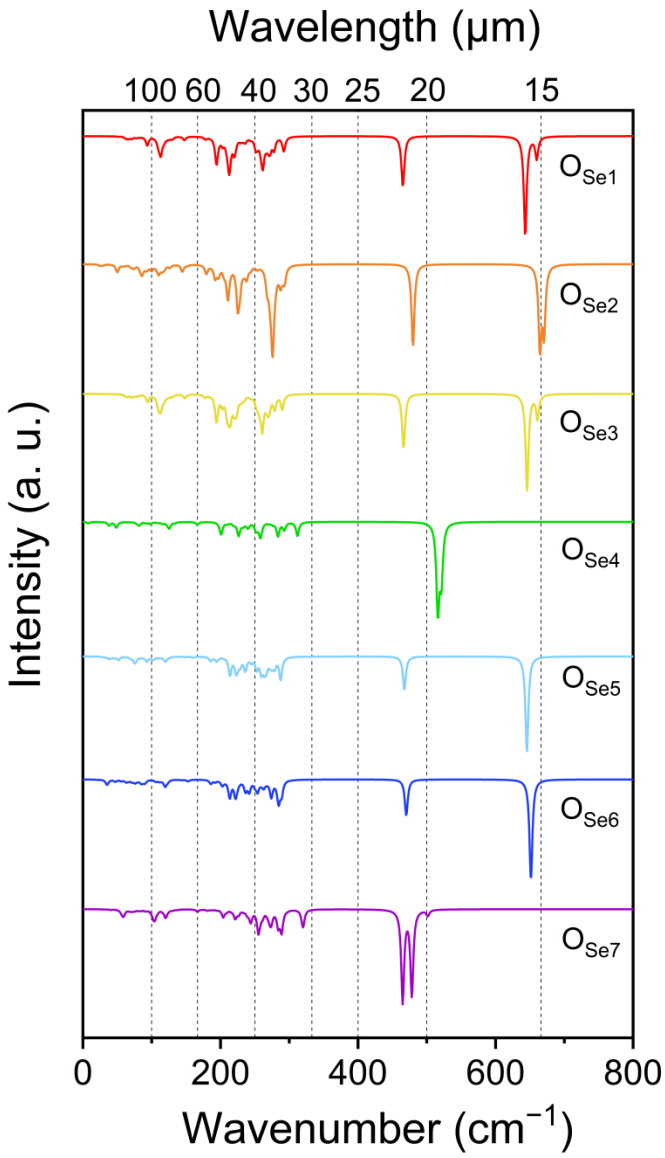

Figure S6. Computational IR spectra for seven O_{Se} defect crystals.

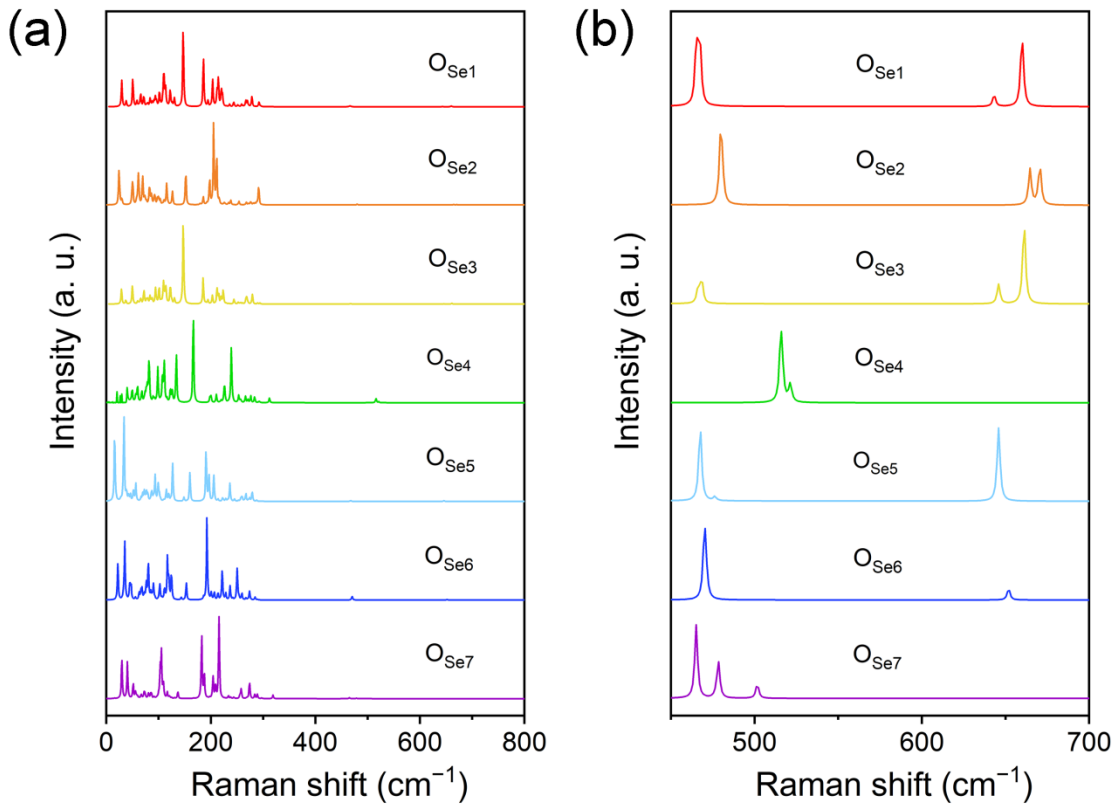

Figure S7. Computational Raman spectra for seven O_{Se} defect crystals in the range of (a) 0−800 cm^{-1} and (b) 450−700 cm^{-1}.